PNAS RESEARCH ARTICLE | PHYSIOLOGY

Structural OFF/ON transitions of myosin in relaxed porcine myocardium predict calcium-activated force

Weikang Ma[a,1], Timothy S. McMillen[b], Matthew Carter Childers[b], Henry Gong[a], Michael Regnier[b], and Thomas Irving[a]

Edited by Edwin Taylor, University of Chicago, Chicago, IL; received May 3, 2022; accepted December 6, 2022

Contraction in striated muscle is initiated by calcium binding to troponin complexes, but it is now understood that dynamic transition of myosin between resting, ordered OFF states on thick filaments and active, disordered ON states that can bind to thin filaments is critical in regulating muscle contractility. These structural OFF to ON transitions of myosin are widely assumed to correspond to transitions from the biochemically defined, energy-sparing, super-relaxed (SRX) state to the higher ATPase disordered-relaxed (DRX) state. Here we examined the effect of 2'-deoxy-ATP (dATP), a naturally occurring energy substrate for myosin, on the structural OFF to ON transitions of myosin motors in porcine cardiac muscle thick filaments. Small-angle X-ray diffraction revealed that titrating dATP in relaxation solutions progressively moves the myosin heads from ordered OFF states on the thick filament backbone to disordered ON states closer to thin filaments. Importantly, we found that the structural OFF to ON transitions are not equivalent to the biochemically defined SRX to DRX transitions and that the dATP-induced structural OFF to ON transitions of myosin motors in relaxed muscle are strongly correlated with submaximal force augmentation by dATP. These results indicate that structural OFF to ON transitions of myosin in relaxed muscle can predict the level of force attained in calcium-activated cardiac muscle. Computational modeling and stiffness measurements suggest a final step in the OFF to ON transition may involve a subset of DRX myosins that form weakly bound cross-bridges prior to becoming active force-producing cross-bridges.

thick filament regulation | X-ray diffraction | dATP | weak binding

Significance

The classical view of muscle regulation is thin filament-based. However, transitions of thick filament myosin motors between ordered OFF states and disordered ON states also now appear to be critical in regulating muscle contractility. Here we used 2'-deoxy-ATP (dATP) to demonstrate how these OFF/ON transitions affect the amount of isometric force by facilitating structural OFF to ON transitions in relaxed muscle. We also show that a population of ON heads can interact weakly with actin, that this population increases with increasing dATP, and that weak binding may represent a necessary step in muscle activation. These insights suggest that both OFF to ON transitions and weak binding events should be considered when designing pharmaceutical interventions targeting contractile properties inside the sarcomere.

Muscle contraction is achieved by cyclic interactions between thick filament myosin and thin filament actin in sarcomeres, the basic structure-function unit of muscle. Contraction is initiated when calcium (Ca^{2+}) binds to the troponin complexes of thin filaments (1, 2), triggering a cascade of conformational changes that increase the mobility of tropomyosin. This exposes myosin-binding sites on the thin filament, allowing myosin heads to attach (cross-bridge formation) and generate force or shortening (3, 4). In relaxed muscle, a portion of the myosin heads in sarcomeres exist in a disordered-relaxed (DRX) state, defined by a relatively high ATPase activity (~0.03 s^{-1}), and the remainder of the myosin heads is sequestered in the super-relaxed (SRX) state with very low ATPase activity (~0.003 s^{-1}) (5–8). The classical thin filament-based scheme for contractile activation and relaxation has now been supplemented with the proposition that dynamic transitions between the energy-sparing SRX states and the more active DRX states of myosin are also involved in regulating muscle contractility (9, 10). These SRX to DRX transitions have been proposed to be the biochemical basis of the structural OFF to ON transitions detected by X-ray diffraction (11). In resting muscle, a large percentage of myosin heads are in the structurally defined quasi-helically ordered OFF state in which myosin motors arranged on the surface of the thick filament give rise to myosin-based layer line reflections in the X-ray diffraction patterns. This helical ordering is lost when myosin heads are turned ON to participate in contraction (12–14). The structural aspects of thick filament regulation were brought to the forefront by Linari et al. (13), who proposed a "mechano-sensing" model for vertebrate muscle thick filament regulation. They proposed that once thin filaments are turned ON, a small number of constitutively ON myosin heads generate a strain on the thick filament backbone, resulting in more myosin heads in the OFF state converting to an active ON state. Whether the biochemically defined SRX to DRX transition reflects the same underlying phenomenon as the structurally defined OFF to ON transition is not yet clear.

The nucleotide 2'-deoxy-ATP (dATP) is a naturally occurring energy substrate for myosin that enhances cross-bridge binding and cycling kinetics (15, 16). In relaxed rodent cardiac and skeletal muscle, dATP repositions myosin heads away from the thick filament backbone and toward the thin filaments (17, 18). A recent report by Walklate et al. (8) quantified the effects of dATP in promoting SRX to DRX transitions in con-contracting myofibrils. The study showed that 100% dATP is sufficient to release all myosin heads

Author contributions: W.M., M.R., and T.I. designed research; W.M., T.S.M., M.C.C., and H.G. performed research; W.M., M.R., and T.I. contributed new reagents/analytic tools; W.M., T.S.M., and M.C.C. analyzed data; and W.M., T.S.M., M.C.C., M.R., and T.I. wrote the paper.

Competing interest statement: The authors have organizational affiliations to disclose, T.I. provides consulting to Edgewise Therapeutics and has collaborative research agreements with Bristol Myers Squibb (formerly MyoKardia), but such work is unrelated to the content of this article.

This article is a PNAS Direct Submission.

[1]To whom correspondence may be addressed. Email: wma6@iit.edu.

This article contains supporting information online at https://www.pnas.org/lookup/suppl/doi:10.1073/pnas.2207615120/-/DCSupplemental.

Published January 25, 2023.

from the SRX state to DRX states in the porcine ventricle muscle. These data demonstrate that dATP is a useful tool for the quantitative assessment of the recruitment of myosin heads from inactive (OFF) to active (ON) states in thick filament activation. Here, we titrated permeabilized porcine myocardium in the relaxed state with dATP to show, using small-angle X-ray fiber diffraction and mechanical assays, that the degree of the transition from the structurally defined ordered OFF state(s) to the disordered ON state(s) is a strong predictor of mechanical output. By comparison with our recent study of SRX/DRX populations of ATP vs. dATP (8), we show that these biochemically defined states are not equivalent to the structurally defined OFF to ON states measured here. Our modeling studies provide an atomic-scale mechanistic basis for the electrostatic recruitment of disordered ON-state myosin heads to become weakly bound prior to becoming active force-producing cross-bridges.

Results

Radial Movement of Myosin Heads. We studied X-ray diffraction patterns from relaxed permeabilized porcine myocardium where the ratio in mixtures of dATP to ATP in solutions ranged from 0 to 100% dATP with the total nucleotide triphosphate (NTP) concentration (dATP + ATP) held constant at 2.5 mM. Example patterns for different mixtures of dATP and ATP are shown in Fig. 1. Permeabilized porcine myocardium in the absence of dATP or at low dATP concentration showed characteristic relaxed X-ray diffraction patterns, similar to those shown in previous studies (19, 20). The equatorial intensity ratio ($I_{1,1}/I_{1,0}$) is widely used as an indicator of the proximity of myosin heads to actin in relaxed muscle (14, 17, 21). $I_{1,1}/I_{1,0}$ was plotted as a function of percent dATP composition and $I_{1,1}/I_{1,0}$ increased continuously as dATP concentrations increased (Fig. 2*A* and *SI Appendix*, Table S1). The increase of $I_{1,1}/I_{1,0}$ indicates a shift of mass, in the form of the myosin S1 heads, away from the thick filament backbone toward the thin filament as dATP concentration increases. $I_{1,1}/I_{1,0}$ as a function of dATP concentrations fitted to an exponential functions ($R^2 = 0.63$) yielded half-concentrations of 11.29% (95% confidence level (CI) 7.0 to 24.5%). The radius of the center of mass of the helically ordered cross-bridges (R_m) to the thick filament backbone can be estimated from the position of the first maxima on the first myosin layer line (MLL1) (22, 23). R_m initially increased ~5% between 0% and 2% dATP followed by a decrease back to its initial value at higher dATP concentrations (Fig. 2*B* and *SI Appendix*, Table S1).

OFF to ON Transitions in Myosin Heads. The majority of myosin heads are quasi-helically ordered on the surface of the thick filament in resting muscle and are unavailable to bind to actin. These myosin heads, in the OFF state, produce the characteristic myosin-based layer line reflections (22). Myosin heads need to be turned ON in order to be able to participate in contraction. Here, we are defining the structural OFF to ON transition based on the mechano-sensing model of (13). The first step of thick filament activation is the development of strain in the thick filament backbone as evidenced by increases of the M6 meridional reflection spacing (S_{M6}), followed by a reduction in the degree of helical ordering of the myosin heads characteristic of the OFF state. Both I_{MLL1} and I_{M3}, indicators of helical ordering of the myosin heads, decreased monotonically with increasing dATP concentration in relaxed muscle, initially rapidly and then leveling off at about 40% of their initial values (*SI Appendix*, Table S1). There were no significant differences in I_{MLL1} ($P = 0.99$) and I_{M3} ($P = 0.82$) between 25% and 100% dATP, suggesting that most of the structural changes have occurred at ≤25% dATP (*SI Appendix*, Table S1). Since the diffracted intensity is proportional to the square of the total electron density, the square root of I_{MLL1} ($\sqrt{I_{MLL1}}$) and I_{M3} ($\sqrt{I_{M3}}$) should be directly correlated to the number of diffracting myosin heads. $\sqrt{I_{MLL1}}$ (Fig. 3*A*) and $\sqrt{I_{M3}}$ (Fig. 3*B*) as a function of dATP composition were fit with one-phase exponential decay functions ($R^2 = 0.60$ and $R^2 = 0.70$, respectively) yielding half-concentrations of 7.4% (95% CI 3.7 to 13.9%), 7.8% (95% CI 4.0 to 14.3%) respectively. S_{M6} increased monotonically with increasing dATP concentration, leveling off at a 0.38% increase from their initial values so that there were no significant differences in S_{M6} between 25% and 100% dATP ($P = 0.99$) (Fig. 3*C* and *SI Appendix*, Table S1). S_{M6} as a function of dATP concentrations fitted to an exponential function ($R^2 = 0.68$) yielded half-concentrations of 5.88% (95% CI 3.0 to 10.3%).

Contractility of Porcine Myocardium in the Presence of dATP. Mechanical studies were performed to investigate whether the observed structural OFF to ON transitions in relaxed muscle can be translated to functional differences in force development upon Ca^{2+} activation. The isometric tension in response to different calcium concentrations was assessed in the presence of 100% ATP or dATP (Fig. 4*A* and *SI Appendix*, Table S2). Maximal tension (pCa 4.0) increased modestly (~11%) with 100% dATP, and a leftward shift of the tension-pCa curve demonstrates a small but significant increase in pCa_{50} (Fig. 4*A* and *SI Appendix*, Table S2), indicating increased calcium sensitivity in the presence of 100% dATP. The passive tension increased from 0 at 100% ATP to 5.2 ± 1.6 mN/mm^2 at 100% dATP. Relative stiffness, measured with low amplitude, high-frequency oscillations (*Methods*) under steady-state force measurement conditions, was linearly related to relative force with increasing Ca^{2+}, and the plots were indistinguishable

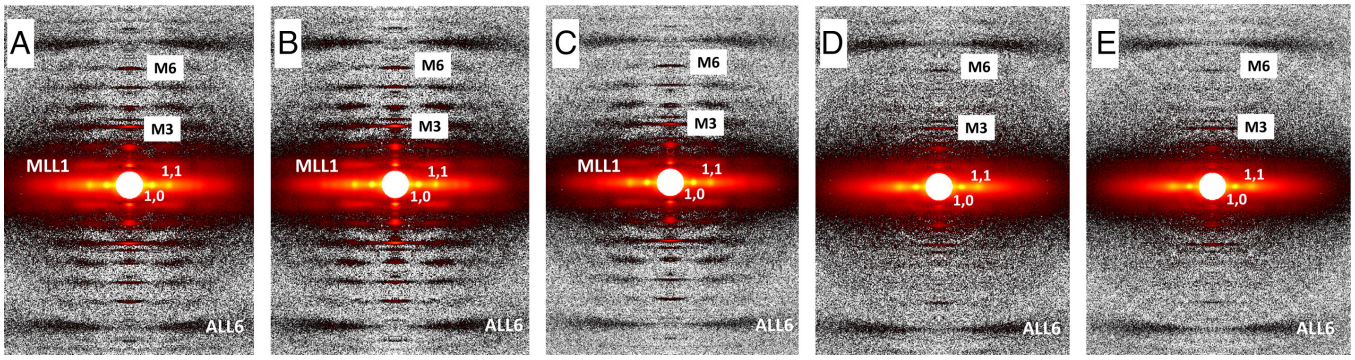

Fig. 1. X-ray diffraction patterns from permeabilized porcine myocardium in relaxing solution as a function of dATP composition. From panel *A* to panel *E*, dATP comprised 0%, 2%, 10%, 25%, and 100%, respectively, of the total nucleotide pool.

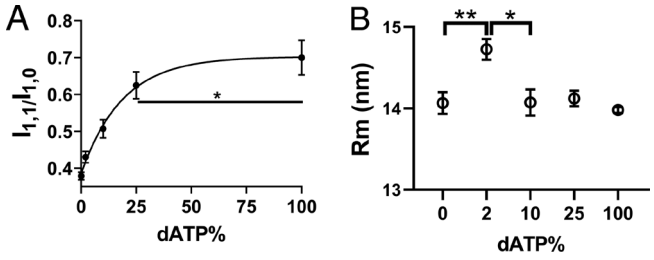

Fig. 2. Radial movement of myosin heads in the presence of dATP. *A*, Equatorial intensity ratio ($I_{1,1}/I_{1,0}$) as a function of dATP composition and one-phase exponential fits to the data. *B*, The radius of average mass of myosin heads (Rm) at different concentration of dATP. Myosin heads moves radially closer to actin as dATP concentration increases. * $P < 0.05$, ** $P < 0.01$.

among preparations at different dATP concentrations (Fig. 4*B* and *SI Appendix*, Table S3). This suggests that dATP does not alter intrinsic properties of the cross-bridges and the increase in force with dATP likely results from proportional increases in the number of strongly bound, cycling cross-bridges (24–26). We then investigated porcine myocardium contractility at intermediate (pCa 5.7) and maximum (pCa 4) calcium concentrations to examine the relative increase in force by dATP. The force augmentation by dATP plateaus at about a 50% increase at 25% dATP at pCa 5.7 (Fig. 4*C*), strongly resembling the structural changes induced by dATP (Fig. 2*A* and Fig. 3). Fits yielded a half-value of 10.28% (95% CI 6.7 to 15.4%) when fit to a one-phase association function (R^2 = 0.75). The relative maximum force at pCa 4.0 increased ~8% at 25% dATP and further increased to 15% at 100% dATP, but this difference was not significant (P = 0.44). Fits (R^2 = 0.75) yielded a half-value of 24.6% (95% CI 12.1 to 139.6%) at pCa 4 (Fig. 4*D*). Interestingly, while most of the structural changes are complete by 25% dATP, $I_{1,1}/I_{1,0}$ continues to increase when dATP concentration is increased to 100%. To further investigate this, paired t tests were performed between 25% and 100% dATP and the $\sqrt{I}_{MLL1}$, $\sqrt{I}_{M3,}$ and S_{M6} values (Fig. 3 *B*–*D*) show no significant differences, while $I_{1,1}/I_{1,0}$ continues to increase significantly (Fig. 2*A*). This suggests further movement of disordered heads toward thin filaments.

Structural Effects of dATP/dADP on Thick/Thin Filament Interactions. Molecular dynamics (MD) simulations of pre-powerstroke (myosin + (d)ADP.Pi) bovine-myosin (*SI Appendix*, Fig. S1*A*) were performed to explore the effects of dADP.Pi on myosin conformation at the molecular and atomic levels. Replacement of ADP.Pi with dADP.Pi led to a series of structural changes that propagated from the nucleotide binding pocket and modulated the conformational distribution of residues in two functional sites: the actin-binding interface and loop 2. The average solvent accessible surface area (SASA) of the actin-binding interface increased from 3,182 Å^2 for myosin+ADP.P_i to 3,271 Å^2 for myosin+dADP.P_i simulations (Fig. 5*A*). The average SASA of loop 2 residues increased from 1,453 Å^2 for myosin+ADP.P_i to 1,609 Å^2 for myosin+dADP.P_i simulations (Fig. 5*B*). These regions of myosin contain many charged amino acids which contribute to the formation and stabilization of the actomyosin complex.

DelPhi and *DelPhiForce* were used to explore how electrostatic interactions can affect myosin OFF to ON transitions at the atomic level. Twenty snapshots were selected from our MD trajectories: 10 each from the myosin+ADP.P_i and myosin+dADP.P_i simulations (Fig. 5*C*). The snapshots were chosen to maximize conformational variability within the representative (i.e., average) SASA distributions of residues in loop 2 and the actin-binding interface. The MD-derived myosin snapshots were oriented against a myosin-binding site of an actin tetramer and then shifted either 20 Å or 30 Å away from the actin surface (*SI Appendix*, Fig. S1*D*). *DelPhiForce* was used to calculate the net electrostatic force exerted by the actin tetramer on the myosin. We found that at the 20 Å separation distance, the force exerted on the myosin+dADP.P_i snapshots was greater than that exerted on the myosin+ADP.P_i snapshots (39.1 ± 6.2 pN vs. 19.3 ± 2.5 pN, P = 0.006; Fig. 5*C*). Since both the magnitude and the direction of the electrostatic force contribute to actomyosin association, we calculated the cosine similarity of the net force vectors and the negative vector that was used to shift myosin away from actin (henceforth called the shift vector). The net force and shift vectors had average cosine similarities of 0.70 and 0.78 for the myosin+dADP.P_i and myosin+ADP.P_i snapshots, respectively. The remaining components of the net force vectors were oriented toward the barbed and/or pointed ends of the actin tetramer. At the 30 Å separation distance, these trends held and the force exerted on the myosin+dADP.P_i snapshots was greater than that exerted on the myosin+ADP.P_i snapshots (9.9 ± 1.2 pN vs. 6.2 ± 0.8 pN, P = 0.02). The net force and shift vectors had average cosine similarities of 0.81 and 0.92 for the myosin+ADP.P_i and myosin+dADP.P_i snapshots, respectively (Fig. 5*D*). At both separation distances, four regions in myosin experienced associative forces (in decreasing order of force magnitude): the helix-loop-helix motif of the lower 50 kDa domain (residues 518 to 556), loop 2 (residues 622 to 645), the cardiomyopathy loop (residues 401 to 416), and loop 4 (residues 362 to 378). Based on visual inspection of the electrostatic potential and the distribution of forces assigned to individual residues, we identified sets of specific residues in myosin for which the associative forces were strongest: K405 (cardiomyopathy loop), K542, K549, K551 (helix-loop-helix motif), K633, and K635 (loop 2). The highly negatively charged N terminus of actin (residues 3 to 6, 26, and 27) contributed most to electrostatic interactions with myosin (Fig. 5 *E* and *F*).

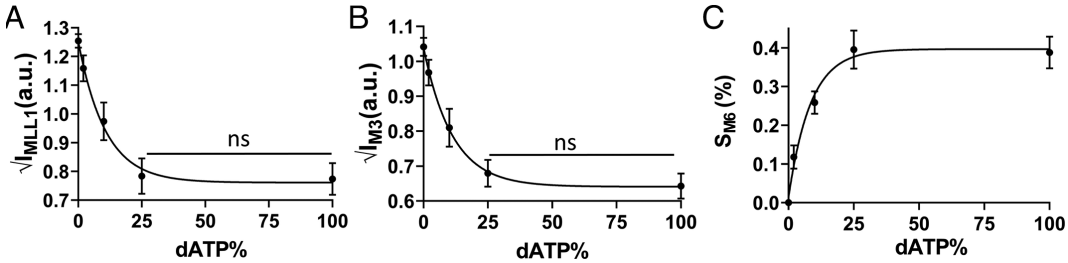

Fig. 3. Thick filament structural changes in the presence of dATP. *A*, Square root of the intensity of the first-order myosin-based layer line ($\sqrt{I}_{MLL1}$) as a function of dATP composition. *B*, Square root of the third order of myosin-based meridional reflection ($\sqrt{I}_{M3}$) as a function of dATP composition. *C*, The spacing of the sixth order of myosin-based meridional reflection (S_{M6}) as a function of dATP composition. The data were fitted to a one-phase exponential function. Myosin heads move from the helically ordered OFF states to disordered ON states as dATP concentration increases. ns: not significant ($P > 0.05$).

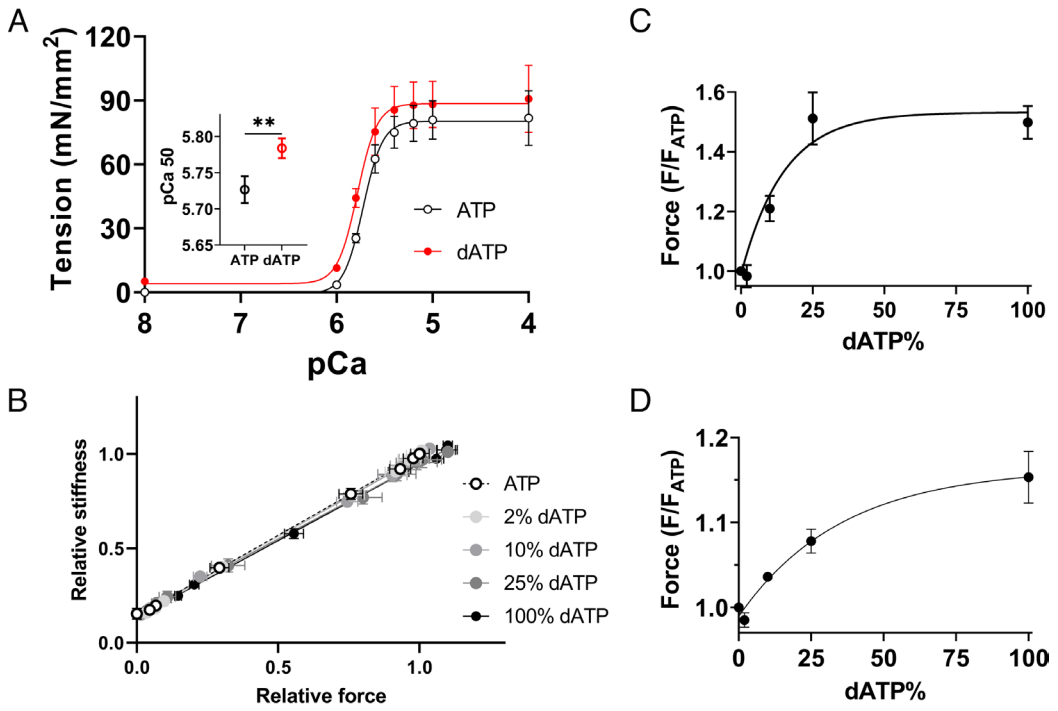

Fig. 4. Contractility of porcine myocardium in the presence of dATP. *A*. Tension as a function of different concentration of calcium (pCa) in the presence of ATP and dATP (*Inset*: pCa 50 of tension). *B*, Stiffness normalized to values at pCa 4 in 0% dATP (*SI Appendix*, Table S3) as a function of relative force at different concentrations of dATP, as force is varied by changes in pCa from 8 to 4. Relative force (normalized to that in 0% dATP) at pCa 5.7 (*C*) and pCa 4 (*D*) as a function of dATP composition and one-phase exponential fits to the data.** $P < 0.01$.

To determine if increased electrostatic interactions between myosin and actin could have an effect even at 2% dATP, where significant increases in $I_{1,1}/I_{1,0}$ (Fig. 2*A*) are already seen, we measured porcine ventricular muscle stiffness at pCa 8.0 for 0% dATP, then 2% dATP (Fig. 6*A*). In pCa 8 solution, which does not elicit thin filament activation nor the active component of force, switching from 0 to 2% dATP results in a significant increase in relative muscle stiffness (1.25 ± 0.05, $P = 0.006$). This suggests that 2% dATP induced some interaction between myosin and actin in sarcomeres. To demonstrate that this increase was due to myosin cross-bridges, in another set of muscle preparations we first compared stiffness in 0% dATP, then 2% dATP, then finally 2% dATP plus the myosin inhibitor 2,3-Butanedione monoxime (BDM). In each of these preparations, relative stiffness was increased with 2% dATP (1.19 ± 0.07, compared with 0%), then significantly decreased (0.89 ± 0.03, $P = 0.014$) by the addition of BDM (Fig. 6*B*). The elevation of stiffness in non-contracting muscle has been interpreted as an increase in weak myosin binding to actin (via electrostatic interactions) and inhibition of stiffness with BDM as a loss of weak binding cross-bridges (24).

Discussion

Structural OFF to ON Transitions Are not Equivalent to Biochemical SRX to DRX Transitions. In relaxed, demembranated rodent cardiac muscle, we have shown that dATP shifts the distribution of myosin heads away from the thick filament backbone toward the thin filaments with 100% dATP (18). We have reported that this also occurs in intact soleus muscle of transgenic mice that over-express ribonucleotide reductase (the enzyme that converts ATP to dATP), where dATP levels are only 1% of the total ATP (17). Here, we report that in porcine left ventricle myocardium where β-myosin is predominantly expressed, as the percentage of dATP in the total nucleotide pool (2.5 mM) increases from 0 to 100%, myosin heads progressively move away from the thick filament backbone toward thin filaments (Fig. 2). At the same time, myosin heads lose their quasi-helical ordering (Figs. 1 and 3) and the thick filament backbone elongates, both indicators that myosin heads undergo the structural OFF to ON transition when they bind dATP. Interestingly, most of the structural transitions ($\sqrt{I_{MLL1}}$, $\sqrt{I_{M3,}}$ and S_{M6} in Fig. 3) reached a maximum at 25% dATP, while the $I_{1,1}/I_{1,0}$ (Fig. 2*A*) continued to increase from 25 to 100%. This further increase in $I_{1,1}/I_{1,0}$ with no change in $\sqrt{I_{MLL1}}$, $\sqrt{I_{M3,}}$ or S_{M6}, strongly suggests a further shift in the disordered myosin heads toward the thin filaments.

While Stewart et al. showed (27) temperature dependence of the SRX/DRX ratio in rabbit skeletal muscle, Walklate et al. reported (8) that the populations of myosin heads in the SRX state were relatively stable in porcine ventricle muscle, as studied here, from 10 °C to 30 °C. We can, therefore, compare the structural findings in this report at 28 °C to 30 °C directly to the SRX/DRX results in Walklate et al. at 20 °C (8). It should be noted, however, that the SRX/RDX results by Walklate et al. (8) were obtained from unloaded myofibril preparations, while our structural results were obtained from myocardium fiber bundles under loaded conditions. The discrepancies in the literature and the different conditions under which the various experiments were conducted, however, suggest that caution should be used in quantitative comparisons of biochemical SRX/DRX ratios obtained by different groups to structural OFF to ON transitions. We replotted the population of myosin heads in SRX state reported by Walklate et al. (8) at each different percentage dATP and the profile is clearly different from that of the structural changes induced by different percentage of dATP (Fig. 7*B*). Our X-ray diffraction data show that the residual I_{MLL1} at 100% dATP is ~40% of the resting value (Fig. 3*A*). This would imply a substantial number of myosin heads remain in a quasi-helically ordered state(s) at 100% dATP. Walklate et al. (8), however, reported that no myosin heads remained in the SRX at 100% dATP, indicating that helically ordered heads are not necessarily in the biochemically defined

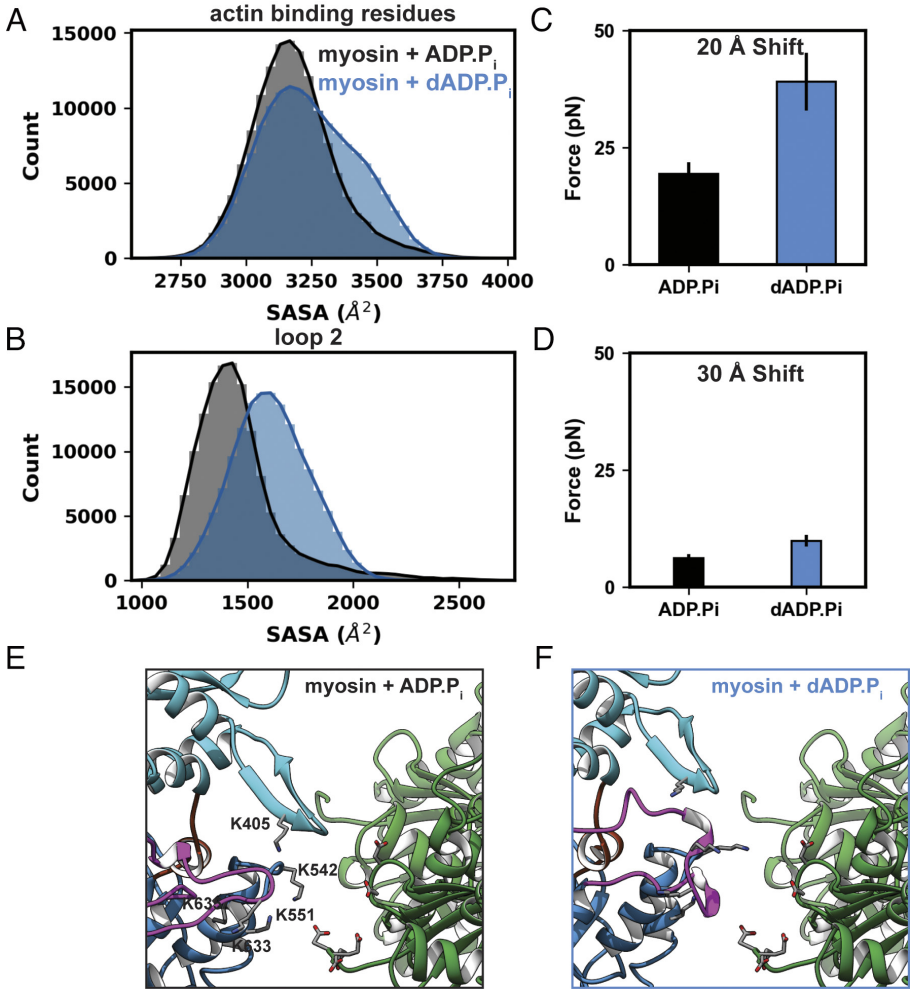

Fig. 5. Replacement of ADP.P$_i$ with dADP.P$_i$ leads to stronger electrostatic interactions between actin and myosin. *A*, Residues in the actin-binding surface of myosin are dynamic and sampled a range of conformations in MD simulations. The histograms show the distributions of the SASA of all actin-binding residues in the myosin+ADP.P$_i$ (black) myosin+dADP.P$_i$ (blue) simulations. *B*, Residues in loop 2 were similarly dynamic and had greater SASA in the myosin+dADP.P$_i$ (blue) simulations. In *DelPhiForce* calculations, actin exerted a greater net electrostatic force on the myosin+dADP.P$_i$ (blue) structures than on the myosin+ADP.P$_i$ (black) structures at shift distances of both 20 Å (*C*) and 30 Å (*D*). Representative, close-up snapshots of the (*E*) myosin+ADP.P$_i$ and (*F*) myosin+dADP.P$_i$ actomyosin complexes. The charged residues that contributed most to actin-myosin electrostatic interactions are shown as sticks and myosin residues are labeled.

SRX state (28). The residual I_{MLL1} remaining is the same at both 25% and 100% dATP (~40%). This would imply a similar number of myosin heads remaining in the helically ordered state at 25% and 100% dATP, while the population of myosin heads in the SRX state decreased (from 25 to 0%). This may indicate that myosin heads in the biochemically defined SRX state do not necessarily need to be helically ordered and that myosin heads in the biochemically defined DRX state are not necessarily structurally disordered. Together, these findings demonstrate that the biochemical SRX/DRX and structural OFF/ON indices do not behave in the same way in response to increasing dATP concentration, and, therefore, they represent different underlying phenomena even though the two processes have been shown to be correlated in some cases (29).

Our definition of OFF state myosin heads does not directly address the precise configuration, and the possible heterogeneity, of the helically ordered heads under relaxed conditions. Under relaxing conditions, two heads in the "canonical" IHM configuration (30), a fixed conformation with two heads folded back onto the thick filament backbone, can form two helices with the free heads forming one helix at larger radius with the blocked heads forming another helix at a smaller radius. Previous modeling studies on tarantula (31) and bony fish (32) skeletal muscles showed that modeling the intensity distribution of myosin layer lines from X-ray diffraction patterns assuming that the heads were in this "canonical" IHM configuration could provide good fits of the predicted to observed intensity distributions. Padron and Craig have more recently clarified the definition of the IHM to encompass a range of structures involving free and blocked heads (29, 30). Here we showed that R_m increased initially as dATP concentration increases to 2% and then reduced back to its original values at higher dATP concentrations (Fig. 2*B* and *SI Appendix*, Table S1). Our results could be explained if there was a transition between helically ordered pairs of heads that initially move radially outward together, while remaining helically ordered, when dATP concentration is low (up to 2% dATP), to pairs consisting of one free head that is disordered and one blocked head that remain helically ordered at a lower radius (31, 33), at higher dATP concentrations. Other explanations are possible. Given the possible heterogeneous nature of relaxed head configurations, one should be cautious in assuming that helically ordered OFF heads are necessarily in the canonical IHM state under all conditions in porcine myocardium.

Degree of dATP-Induced Disordering of Myosin Heads in Relaxed Muscle Predict Force Output in Active Muscle. An expression for the ensemble force (F_{ens}) generated by the cross-bridges in

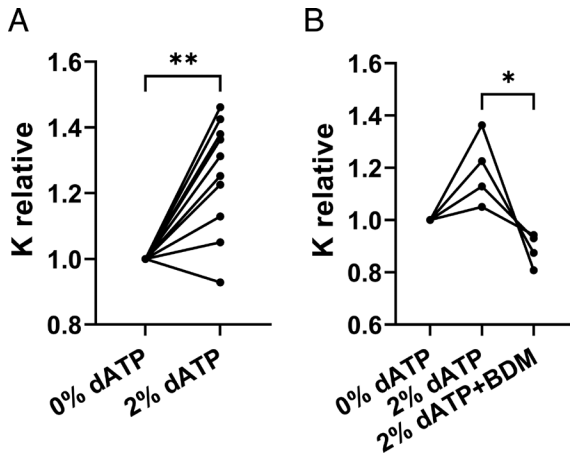

Fig. 6. dATP enhances weak myosin binding in porcine myocardium. *A*, High-frequency sinusoidal stiffness was measured at pCa 8 first in ATP then in 2% dATP (n = 9), *B*, In a separate set of experiments (n = 4), stiffness was measured in ATP, then 2% dATP followed by 2% dATP plus BDM (30 mM). Relative stiffness was normalized to stiffness at 0% dATP (*SI Appendix*, Table S3). * $P < 0.05$, ** $P < 0.01$

a sarcomere has been elegantly formulated by Spudich as $F_{ens} = F_{int} \cdot N_a \cdot t_s/t_c$, where F_{int} is the intrinsic force of a powerstroke, N_a is the number of functionally accessible heads that binds actin during contraction, and t_s/t_c is the duty ratio, i.e., the proportion of the ATPase cycle that the motor domain remains strongly bound to actin (10). Changes in any of, or any combination of, these three parameters will affect the ensemble force generated by the sarcomere. Implicit in the concept of thick filament activation is that the process primarily alters N_a rather than F_{int} or t_s/t_c. Relative stiffness (Fig. 4*B*) was linearly related to relative force with increasing Ca^{2+}, suggesting dATP did not affect the intrinsic force production per cross-bridge. This suggests that any changes in muscle isometric force development caused by dATP (in activation solutions) were due to changes in the number of force-generating cross-bridges (N_a). It has been shown that the binding affinity of dATP for cardiac beta myosin is similar to that for ATP (34), so we assume that the percentage of myosin heads bound to dATP is approximately proportional to the percentage of dATP in the total nucleotide pool. Walklate et al. (8) reported that at 20 °C, the population of myosin heads in the SRX state decreases linearly as dATP concentration increases in porcine ventricle muscle. The X-ray data show, however, that the structural changes of myosin heads induced by dATP have already occurred with 25% of the NTP pool being dATP (Figs. 2*A* and 3). Similarly, the degree of force elevation, at least at submaximal calcium concentration, also plateaus at ~25% dATP composition (Fig. 4*C*). In Fig. 7*A*, we show that any of the relative changes in the structural parameters plotted as a function of relative force yields a linear relationship with correlation coefficients for all structural parameters ($R^2 > 0.9$). This high degree of correlation implies that the dATP-induced configuration of myosin heads in the relaxed muscle is a strong predictor of subsequent tension development.

Thick Filament Activation does not End at the DRX State. The increase in myosin heads in the DRX state is proportional (linear) with increasing % dATP (8), but the increase in isometric force generation (Fig. 4*C*) is a nonlinear function of dATP % of the nucleotide content, suggesting that not all DRX myosin heads have the same probability of recruitment to the pool of actively cycling cross-bridges during contraction in cardiac muscle. We previously reported that dATP changes the structure of the myosin S1 head (17, 18, 35), such that there is an increase in the electrostatic affinity for actin that results in S1 being drawn toward the thin filaments in relaxed sarcomeres (18). Our previous studies have mostly examined relaxed and contracting muscle comparing 100% ATP vs. 100% dATP. However, in a recent study (17) of soleus muscle from transgenic mice that over-express ribonucleotide reductase (RNR), resulting in dATP being increased to ~1% of the total nucleotide pool, we reported that myosin stays closer to actin following relaxation from tetanus. Here, using bathing solutions with different ratios of dATP to ATP (with the total nucleotide held constant), our data show that just 2% dATP is sufficient to result in significant movement of myosin toward thin filaments indicating that structural transitions in one head appear to induce transitions in neighboring heads, so that the relationship of structural transitions to dATP concentrations is nonlinear, saturating at 25% dATP. To explore the effects of dADP on myosin conformation, MD simulations of pre-powerstroke bovine β-myosin+(d)ADP.Pi were performed. The results presented here were consistent with prior findings in *Dictyostelium discoideum* (slime mold) and *Argopecten irradians* (scallop) myosin II MD simulations (17, 18, 36, 37). Replacement of ADP with dADP led to an increase in the SASA of residues in the actin-binding interface and of residues in loop 2. dADP also promoted the sampling of a broader range of loop 2 conformations. Additionally, we found that actin exerted a greater electrostatic attractive force on myosins from the myosin+dADP.P_i simulations. We attribute this increase in force to structural changes among actin-binding residues of myosin. Even small differences in the total loop 2 surface area led to broad changes in electrostatic interactions between actin and myosin. Based on these results, we have refined our hypothesis to state that by promoting conformations of myosin that are more electrostatically attracted to the thin filament, dATP modulates myosin's conformation to form a structure with greater probability of binding to actin, but

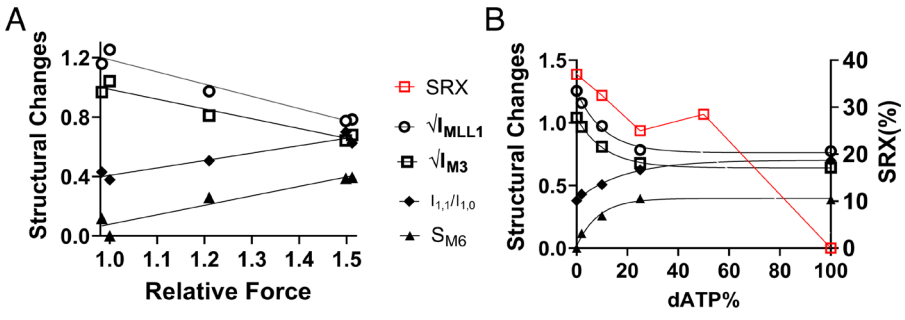

Fig. 7. Force is better correlated with structural ON/OFF than biochemical SRX/DRX transitions with increasing dATP. *A*, The average values of structural changes ($\sqrt{I}_{MLL1}$: hollow circles; $\sqrt{I}_{M3}$: hollow squares; $I_{1,1}/I_{1,0}$: solid diamonds; S_{M6}: solid triangles) as a function of the averaged relative force a. *B*, Structural changes (black symbols, left Y-axis) and percentage of myosin heads in SRX state reported by Walklate et al. (8) (red squares, right Y-axis) in response to different concentrations of dATP.

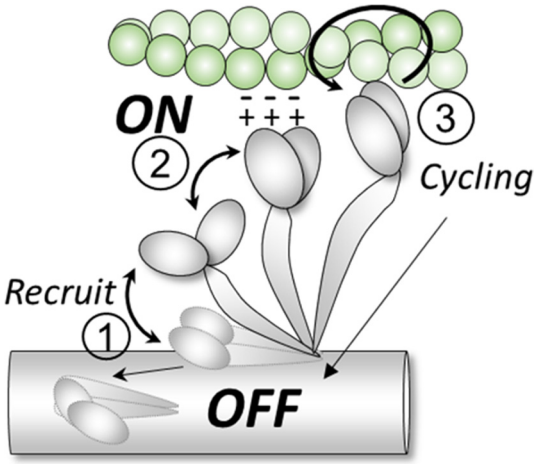

Fig. 8. OFF and ON states of myosin. Under relaxing conditions, the majority of the myosin heads are in the helically ordered OFF state on the surface of the thick filament backbone. Upon recruitment (1), myosin heads move toward the thin filament and become disordered. A portion of the ON heads in close proximity to actin form weak electrostatic interactions with actin molecules (2) that are then more likely to participate in contraction once the binding sites are exposed in the presence of calcium (3).

not necessarily resulting in stronger force of contraction. At 100% dATP, the passive tension increases significantly (*SI Appendix*, Table S2) indicating that dATP-induced increases in actomyosin interactions may increase the probability of transitioning to force bearing states. Our MD simulations also showed weaker, but still significant, electrostatic forces between actin and myosin with ADP.Pi in the nucleotide in binding pocket (Fig. 5 *C* and *D*), indicating that the weakly binding cross-bridges are still present in a purely ATP environment, as shown in previous studies suggesting that weak binding cross-bridges under relaxing conditions are a precursor to strong binding, force-producing cross-bridge (24, 38, 39). Our stiffness measurements in resting porcine ventricle muscle support this hypothesis. Fig. 6*A* shows that stiffness was significantly increased when the relaxing solution was switched from 0 to 2% dATP indicating an increase in weak cross-bridge interactions induced by dATP. The stiffness then significantly decreased to below that of 0% dATP (all ATP) after the addition of BDM, suggesting that weakly binding cross-bridges are indeed present in relaxed muscle with ATP in the bathing solution and that the weak binding cross-bridge mechanism we propose as an additional step in thick filament regulation has broad physiological relevance (24). These results also suggest that not all myosin heads in the biochemically defined DRX state have equal opportunity to form cross-bridges and that a sub-population of DRX myosin interacts weakly with actin. This would be expected to decrease the distance between myosin heads and their binding sites on actin and, thus, increase the probability of cross-bridge formation and cycling during Ca^{2+} activated contractions, and this could explain the observed leftward shift of the force/pCa curve in the presence of dATP (Fig. 4*A*). Future studies will be required to determine the impact of increased weakly bound myosin cross-bridges on the regulation of myofibril contractile kinetics and cardiac muscle twitch dynamics.

Conclusions

It has been generally assumed that the structurally defined order to disorder transition is also the structural basis of the biochemically defined SRX to DRX transitions of myosin. Here in this study, using dATP as a perturbation, we show by comparing with our previous studies of SRX/DRX transitions with dATP (8) that the biochemically defined SRX/DRX transitions are not equivalent to the structurally defined OFF to ON transitions. We showed that the structurally defined order (OFF) to disorder (ON) transitions induced by dATP are strongly correlated with subsequent isometric force development in contracting muscle. Based on our modeling and stiffness measurements, we propose that disordered heads that approach the actin filament are electrostatically attracted to actin and may form weakly bounded cross-bridges under relaxed conditions. Increased numbers of such weakly bound cross-bridges may be expected to facilitate subsequent force generation in the activated state (Fig. 8). Our exploration of the influence of dATP suggests that there is value in exploring whether other sarcomeric modulators work, at least partially, by regulating the proportions of OFF/ON and weakly bound heads providing a new area for optimization of pharmaceutical interventions.

Materials and Methods

X-ray and mechanical experiments were performed using permeabilized porcine left ventricle wall muscle. Briefly, the frozen muscle was thawed in skinning solution at room temperature before dissection into smaller strips and skinned at room temperature for 3 h. Permeabilized fiber bundles were further dissected into preparations with a length of 4 mm with a diameter of 200 μm prior to attachment of aluminum T-clips to both ends for X-ray experiments. X-ray diffraction patterns were collected at BioCAT beamline (40) on a MarCCD 165 detector (Rayonix Inc.) with a 1 s exposure time as a function of five increasing dATP compositions (0%, 2%, 10%, 25%, and 100%) with the total NTP concentration (dATP + ATP) remaining constant at 2.5 mM after 10 min incubation in each solution. The data were analyzed using data reduction programs belonging to the open-source MuscleX software package developed at BioCAT (41). The intensity of the X-ray reflections was normalized against the intensity of the sixth-order actin-based layer line (I_{ALL6}), which remain relatively constant across the dATP titration series (*SI Appendix*, Table S1). For mechanical experiments, thin left ventricular strips (~120 μm wide, ~1 mm long) were attached to a custom-built mechanical apparatus at 28 °C during Ca^{2+} activation at various concentrations in the presence of 2.5 mM ATP or dATP. Stiffness was determined by small amplitude (0.05% Ls) sinusoidal length oscillations (1 kHz), as reported previously (42). Molecular models were built from bovine cardiac myosin II motor domain. Starting coordinates for bovine (Bos taurus) cardiac myosin II motor domain (residues 4 to 810) and essential light chain (residues 39 to 199) in the pre-powerstroke (Myosin + ADP.Pi + Mg2+) state were obtained from an X-ray crystal structure in the Protein Data Bank [PDB, www.rcsb.org (43)] solved by Houdusse et al (PDB ID: 5N69, 2.45 Å resolution) (44). See *SI Appendix, Supplemental Material* for further details.

Data, Materials, and Software Availability. All datasets generated or analyzed for this study are included in this article. The raw X-ray diffraction patterns in this study are deposited at Zenodo repository that available to the public (https://doi.org/10.5281/zenodo.7051303) (45). All other data are included in the manuscript and/or *SI Appendix*.

ACKNOWLEDGMENTS. This research was supported by NIH grant R01 HL128368 (M.R.). This research used resources of the University of Washington Center for Translational Muscle Research, supported by the NIH National Institute of Arthritis and Musculoskeletal and Skin Diseases under Award Number P30AR074990 (M.R.) This research used resources of the Advanced Photon Source, a U.S. Department of Energy (DOE) Office of Science User Facility operated for the DOE Office of Science by Argonne National Laboratory under Contract No. DE-AC02-06CH11357. Use of the BioCAT beamline 18ID is supported by grant P30 GM138395 (T.I.) from the National Institute of General Medical Sciences of the NIH. The content is solely the authors' responsibility and does not necessarily reflect the official views of the National Institute of General Medical Sciences or the NIH.

Author affiliations: [a]Biology, Illinois Institute of Technology, Chicago, IL, 60616; and [b]Bioengineering, University of Washington, Seattle, WA, 98109

1. L. S. Tobacman, Thin filament-mediated regulation of cardiac contraction. *Annu. Rev. Physiol.* **58**, 447–481 (1996).
2. T. Wakabayashi, Mechanism of the calcium-regulation of muscle contraction–in pursuit of its structural basis. *Proc. Jpn. Acad. Ser. B Phys. Biol. Sci.* **91**, 321–350 (2015).
3. W. Lehman, R. Craig, P. Vibert, Ca^{2+} induced tropomyosin movement in *Limulus* thin filaments revealed by three-dimensional reconstruction. *Nature* **368**, 65–67 (1994).
4. Y. Yamada, K. Namba, T. Fujii, Cardiac muscle thin filament structures reveal calcium regulatory mechanism. *Nat. Commun.* **11**, 153 (2020).
5. R. Cooke, The role of the myosin ATPase activity in adaptive thermogenesis by skeletal muscle. *Biophys. Rev.* **3**, 33–45 (2011).
6. P. Hooijman, M. A. Stewart, R. Cooke, A new state of cardiac myosin with very slow ATP turnover: A potential cardioprotective mechanism in the heart. *Biophys. J.* **100**, 1969–1976 (2011).
7. J. W. McNamara, A. Li, C. G. Dos Remedios, R. Cooke, The role of super-relaxed myosin in skeletal and cardiac muscle. *Biophys. Rev.* **7**, 5–14 (2015).
8. J. Walklate, K. Kao, M. Regnier, M. A. Geeves, Exploring the super-relaxed state of myosin in myofibrils from fast-twitch, slow-twitch and cardiac muscle. *J. Biol. Chem.* **293**, 101640 (2022), 10.1016/j.jbc.2022.101640.
9. S. Nag, D. V. Trivedi, To lie or not to lie: Super-relaxing with myosins. *Elife* **10**, e63703 (2021).
10. J. A. Spudich, Three perspectives on the molecular basis of hypercontractility caused by hypertrophic cardiomyopathy mutations. *Pflugers Archiv: Eur. J. Physiol.* **471**, 701–717 (2019).
11. M. Irving, Regulation of contraction by the thick filaments in skeletal muscle. *Biophys. J.* **113**, 2579–2594 (2017).
12. H. E. Huxley, W. Brown, The low-angle X-ray diagram of vertebrate striated muscle and its behaviour during contraction and rigor. *J. Mol. Biol.* **30**, 383–434 (1967).
13. M. Linari *et al.*, Force generation by skeletal muscle is controlled by mechanosensing in myosin filaments. *Nature* **528**, 276–279 (2015).
14. W. Ma, H. Gong, T. Irving, Myosin head configurations in resting and contracting murine skeletal muscle. *Int. J. Mol. Sci.* **19**, 2643 (2018).
15. M. Regnier, D. A. Martyn, P. B. Chase, Calcium regulation of tension redevelopment kinetics with 2-deoxy-ATP or low [ATP] in rabbit skeletal muscle. *Biophys. J.* **74**, 2005–2015 (1998).
16. M. Regnier, A. J. Rivera, Y. Chen, P. B. Chase, 2-deoxy-ATP enhances contractility of rat cardiac muscle. *Circ. Res.* **86**, 1211–1217 (2000).
17. W. Ma *et al.*, Myosin dynamics during relaxation in mouse soleus muscle and modulation by 2′-deoxy-ATP. *J. Physiol.* **598**, 5165–5182 (2020).
18. J. D. Powers *et al.*, Cardiac myosin activation with 2-deoxy-ATP via increased electrostatic interactions with actin. *Proc. Natl. Acad. Sci. U.S.A.* **116**, 11502–11507 (2019).
19. W. Ma *et al.*, The super-relaxed state and length dependent activation in porcine myocardium. *Circ. Res.* **129**, 617–630 (2021).
20. R. L. Anderson *et al.*, Deciphering the super relaxed state of human beta-cardiac myosin and the mode of action of mavacamten from myosin molecules to muscle fibers. *Proc. Natl. Acad. Sci. U.S.A.* **115**, E8143–E8152 (2018).
21. J. C. Haselgrove, H. E. Huxley, X-ray evidence for radial cross-bridge movement and for the sliding filament model in actively contracting skeletal muscle. *J. Mol. Biol.* **77**, 549–568 (1973).
22. W. Ma, T. C. Irving, Small angle X-ray diffraction as a tool for structural characterization of muscle disease. *Int. J. Mol. Sci.* **23**, 3052 (2022).
23. Y. Ait-Mou *et al.*, Titin strain contributes to the Frank-Starling law of the heart by structural rearrangements of both thin- and thick-filament proteins. *Proc. Natl. Acad. Sci. U.S. A.* **113**, 2306–2311 (2016).
24. M. Regnier, C. Morris, E. Homsher, Regulation of the cross-bridge transition from a weakly to strongly bound state in skinned rabbit muscle fibers. *Am. J. Physiol.* **269**, C1532–C1539 (1995).
25. M. Regnier, D. M. Lee, E. Homsher, ATP analogs and muscle contraction: Mechanics and kinetics of nucleoside triphosphate binding and hydrolysis. *Biophys. J.* **74**, 3044–3058 (1998).
26. A. M. Gordon, E. Homsher, M. Regnier, Regulation of contraction in striated muscle. *Physiol. Rev.* **80**, 853–924 (2000).
27. M. A. Stewart, K. Franks-Skiba, S. Chen, R. Cooke, Myosin ATP turnover rate is a mechanism involved in thermogenesis in resting skeletal muscle fibers. *Proc. Natl Acad. Sci. U.S.A.* **107**, 430–435 (2010).
28. C. Wilson, N. Naber, E. Pate, R. Cooke, The myosin inhibitor blebbistatin stabilizes the super-relaxed state in skeletal muscle. *Biophys. J.* **107**, 1637–1646 (2014).
29. R. Craig, R. Padron, Structural basis of the super- and hyper-relaxed states of myosin II. *J. Gen. Physiol.* **154**, e202113012 (2022).
30. R. Padrón, D. Dutta, R. Craig, Variants of the myosin interacting-heads motif. *J. Gen. Physiol.* **155**, e202213249 (2022).
31. R. Padron *et al.*, The myosin interacting-heads motif present in live tarantula muscle explains tetanic and posttetanic phosphorylation mechanisms. *Proc. Natl. Acad. Sci. U.S.A.* **117**, 11865–11874 (2020), 10.1073/pnas.1921312117.
32. N. A. Koubassova *et al.*, Interacting-heads motif explains the X-ray diffraction pattern of relaxed vertebrate skeletal muscle. *Biophys. J.* **121**, 1354–1366 (2022).
33. J. Gu, S. Xu, L. C. Yu, A model of cross-bridge attachment to actin in the A*M*ATP state based on X-ray diffraction from permeabilized rabbit psoas muscle. *Biophys. J.* **82**, 2123–2133 (2002).
34. F. S. Korte *et al.*, Upregulation of cardiomyocyte ribonucleotide reductase increases intracellular 2 deoxy-ATP, contractility, and relaxation. *J. Mol. Cell Cardiol.* **51**, 894–901 (2011).
35. S. G. Nowakowski *et al.*, Transgenic overexpression of ribonucleotide reductase improves cardiac performance. *Proc. Natl. Acad. Sci. U.S.A.* **110**, 6187–6192 (2013).
36. M. C. Childers, M. Geeves, V. Daggett, M. Regnier, Modulation of post-powerstroke dynamics in myosin II by 2′-deoxy-ADP. *Arch. Biochem. Biophys.* **699**, 108733 (2021).
37. S. G. Nowakowski, M. Regnier, V. Daggett, Molecular mechanisms underlying deoxy-ADP. Pi activation of pre-powerstroke myosin. *Protein Sci.* **26**, 749–762 (2017).
38. K. J. Jarvis, K. M. Bell, A. K. Loya, D. M. Swank, S. Walcott, Force-velocity and tension transient measurements from Drosophila jump muscle reveal the necessity of both weakly-bound cross-bridges and series elasticity in models of muscle contraction. *Arch. Biochem. Biophys.* **701**, 108809 (2021).
39. F. Eakins, C. Pinali, A. Gleeson, C. Knupp, J. M. Squire, X-ray diffraction evidence for low force actin-attached and rigor-like cross-bridges in the contractile cycle. *Biology (Basel)* **5**, 41 (2016).
40. R. Fischetti *et al.*, The BioCAT undulator beamline 18ID: A facility for biological non-crystalline diffraction and X-ray absorption spectroscopy at the advanced photon source. *J. Synchrotron Radiat.* **11**, 399–405 (2004).
41. J. Jiratrakanvong *et al.*, MuscleX: Software suite for diffraction X-ray imaging (V1.13.1, 2018). Zenodo. 10.5281/zenodo.1195050. Deposited 21 December 2022.
42. M. Regnier *et al.*, Cross-bridge versus thin filament contributions to the level and rate of force development in cardiac muscle. *Biophys. J.* **87**, 1815–1824 (2004).
43. H. M. Berman *et al.*, The protein data bank. *Nucleic Acids Res.* **28**, 235–242 (2000).
44. V. J. Planelles-Herrero, J. J. Hartman, J. Robert-Paganin, F. I. Malik, A. Houdusse, Mechanistic and structural basis for activation of cardiac myosin force production by omecamtiv mecarbil. *Nat. Commun.* **8**, 190 (2017).
45. W. Ma *et al.*, X-ray diffraction patterns of the effects of dATP on permeabilized porcine myocardium. Zenodo. https://zenodo.org/record/7051303#.Y75Hgv5Bw2w. Deposited 5 September 2022.